


ORIGINAL RESEARCH

Bayesian multipath-enhanced device-free localisation: Simulation- and measurement-based evaluation

Martin Schmidhammer  | Benjamin Siebler | Christian Gentner | Stephan Sand | Uwe-Carsten Fiebig

Institute of Communications and Navigation,
German Aerospace Center (DLR), Wessling,
Germany

Correspondence

Martin Schmidhammer, Institute of
Communications and Navigation, German
Aerospace Center (DLR), Muenchner Str. 20,
Oberpfaffenhofen, 82234 Wessling, Germany.
Email: martin.schmidhammer@dlr.de

Funding information

Open access funding enabled and organized by
Projekt DEAL.

Abstract

Device-free localisation (DFL) systems infer presence and location of moving users by measuring to which extent they change the received signal power in wireless links. Consequently, users not only induce perturbations to the power of the line of sight but also to the power of reflected and scattered signals which are observed in the received signal as multipath components (MPCs). Since the propagation paths of MPCs differ inherently from the line-of-sight path, these propagation paths can be considered as additional network links. This extended network determines the multipath-enhanced device-free localisation (MDFL) system. Based on empirical models that relate perturbations in the received power of MPCs to the user location, the localisation problem can be solved by non-linear Bayesian filtering. In this work, we investigate the point mass filter and the particle filter as possible solutions. We demonstrate the applicability of these solutions using ultra-wideband measurements and develop and verify a numerical simulation framework that flexibly enables a sound evaluation of MDFL. Based on both measurements and simulations, we show a significant improvement of the localisation performance of MDFL compared to DFL. The overall localisation performance is thereby comparable for both filters. Eventually, we show that complexity and divergence probability, rather than localisation performance, are the decisive factors for the choice of the filter solution.

KEYWORDS

Bayes methods, radiowave propagation, ultra-wideband technology, wireless channels, wireless sensor networks

1 | INTRODUCTION

In today's wireless world, smartphones widely use Bluetooth and WLAN as radio technologies for indoor communication covering short to medium range and low to high data rate communications. The scientific community has extensively studied their suitability for indoor localisation and several commercial products exist today to enable indoor localisation [1]. According to Ref. [2], the global indoor location market will grow from \$7.0 billion in 2021 to \$19.7 billion by 2026 with the dominant technologies being WLAN, Bluetooth, and ultra-wideband (UWB). Location dependent measurements range from received signal strength (RSS) to time of flight-

based round trip time measurements [3]. While many use cases require the precise localisation of a person's device, there exist several use cases that need to localise persons without a device [4]. For instance, home security systems aim at detecting the presence of intruders even if they do not carry smartphones. Similarly, a smart climate control for a room needs to detect the presence and number of persons in the room to adjust temperature, humidity and ventilation automatically without requiring any user interaction. Furthermore, a surround sound system should track the location of listeners in a room without requiring manual adjustments every time a listener moves within the room. For addressing this increasing demand in location-aware services, alternative passive

This is an open access article under the terms of the Creative Commons Attribution License, which permits use, distribution and reproduction in any medium, provided the original work is properly cited.

© 2022 The Authors. *IET Microwaves, Antennas & Propagation* published by John Wiley & Sons Ltd on behalf of The Institution of Engineering and Technology.



localisation solutions are required that particularly enable the localisation of users that are not equipped with active localisation devices. Since connectivity, that is, the number of connected devices, is steadily increasing, radio frequency-based passive localisation systems, such as device-free localisation (DFL) [5], are becoming possible solutions.

Current DFL systems infer the presence and location of these non-equipped users by measuring the RSS between network nodes along the line-of-sight (LoS) path. Using empirical propagation models, the DFL system directly relates these RSS measurements to the user location [5–8]. Thereby, the localisation accuracy of such DFL systems improves with the number of network nodes [8]. An increasing number of network nodes, however, results in increasing infrastructural efforts. Motivated by Ref. [9], where we have shown that users also induce variations in the power of multipath components (MPCs), we have proposed in Ref. [10] a novel multipath-enhanced device-free localisation (MDFL) approach, which considers the propagation paths of MPCs as additional network links. For the same amount of networks nodes, MDFL is shown to improve the localisation performance compared to DFL and helps to reduce infrastructural requirements. In Ref. [11], we have presented corresponding non-linear Bayesian filter solutions required to realise MDFL. These filter solutions have been evaluated by simulations. In order to verify the numerical simulation framework used in Ref. [11], we have conducted an indoor measurement campaign as part of this work. In particular, we measured the radio channel with commercial off-the-shelf (COTS) UWB devices, which enable us to derive and verify this numerical simulation framework based on measurements. Thereby, the UWB devices are spatially distributed in an office room and connected to form a network. Based on this setup, we further demonstrate the applicability of the considered filter solutions for an indoor scenario. We apply the filter solutions for both DFL and MDFL and can thus compare the performance of the two systems. Finally, we employ the numerical simulation framework to evaluate the performance of each Bayesian filter solution in detail.

Therewith, the main contributions of this work are as follows:

- the introduction of Bayesian filter solutions for MDFL,
- the implementation of an indoor measurement campaign with COTS UWB devices,
- the development of a numerical simulation framework for MDFL and its verification by measurements,
- the numerical evaluation of Bayesian filter solutions,
- the demonstration and the evaluation of MDFL using measurements.

The remainder of this paper is organised as follows. Preliminaries on MDFL including network, propagation, and measurement model are provided in Section 2. Bayesian localisation approaches are introduced in Section 3 and applied to measured data in Section 4. Based on simulations, the Bayesian localisation approaches are evaluated numerically in Section 5. Finally, Section 6 concludes the paper.

2 | MULTIPATH-ENHANCED DEVICE-FREE LOCALISATION

In this section, we introduce the preliminaries for the novel MDFL approach. Therefore, we present the required network structure and the corresponding terminology. We further specify the propagation model and elaborate the concept of reflection sequences. Finally, we explain the parameter estimation and present the measurement model used for MDFL.

2.1 | Network and propagation model

An MDFL system relies on a network of N_{Tx} transmitting and N_{Rx} receiving nodes, which can be either individually placed, as in the network shown in Figure 1, or collocated, as in the network shown in Figure 4. The locations of the network nodes are thereby assumed to be known at \mathbf{r}_{Tx_i} , $i \in \{1, \dots, N_{\text{Tx}}\}$, and \mathbf{r}_{Rx_j} , $j \in \{1, \dots, N_{\text{Rx}}\}$. For $N_{\text{Tx}} = N_{\text{Rx}} = N$ collocated nodes, that is, transceiving nodes, we can express the node locations also as $\{\mathbf{r}_{\text{TR}_1}, \dots, \mathbf{r}_{\text{TR}_N}\}$, see Figure 4. In either case, a network link l is determined by the i th transmitting and the j th receiving node. For each network link l , the received signal is modelled as a superposition of scaled and delayed replica of a known transmit signal [12]. Due to reflections off the surrounding environment, these replica comprise the LoS component and a finite number of MPCs. Mathematically, the behaviour of the radio channel of link l can be described by the time-variant channel impulse response (CIR) $h_l(t, \tau)$, where t and τ indicate time and delay [13]. Assuming the CIR to be constant for a short time interval, it can be expressed as

$$h_l(t, \tau) = \sum_{n=0}^{N_l-1} \alpha_{l,n}(t) \delta(\tau - \tau_{l,n}), \quad (1)$$

where the variables $\alpha_{l,n}(t)$ and $\tau_{l,n}$ denote the time-variant, complex amplitude and the static propagation delay of the n th component, and $\delta(\cdot)$ represents the Dirac distribution. The CIR considers N_l components, where $n = 0$ refers to the LoS component. Given the CIR of Equation (1), the received signal can be expressed as the convolution of $h_l(t, \tau)$ with a known transmitted signal $s_l(t)$ of duration T_{sym} , that is, as

$$\begin{aligned} y_l(t) &= s_l(t) * h_l(t, \tau) + n_l(t) \\ &= \sum_{n=0}^{N_l-1} \alpha_{l,n}(t) s_l(t - \tau_{l,n}) + n_l(t), \end{aligned} \quad (2)$$

with $n_l(t)$ as additive white circular symmetric normal distributed noise of variance σ_y^2 . Examples of the signal propagation for individual links are highlighted in Figures 1 and 4, both showing the LoS and MPCs due to first-order reflections from the respective surrounding environment.

The idea of MDFL is to use variations in the power of both the LoS component and the MPCs for DFL. In order to extract location information from variations in the power of MPCs, we need to model the corresponding propagation



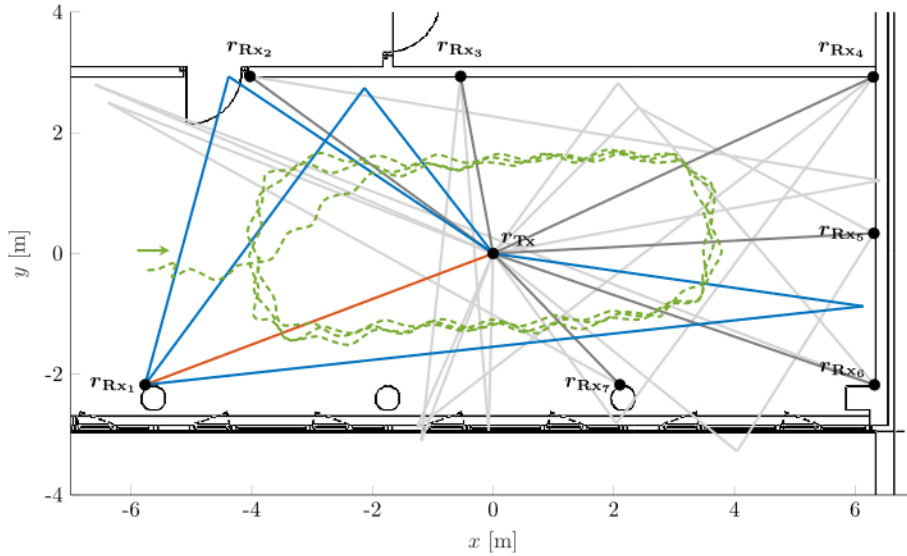


FIGURE 1 Multipath-enhanced device-free localisation network including one transmitting node at \mathbf{r}_{Tx} and several receiving nodes $\mathbf{r}_{\text{Rx}}, j \in \{1, \dots, 7\}$. For the network link between \mathbf{r}_{Tx} and \mathbf{r}_{Rx} , the multipath propagation is explicitly highlighted: physical propagation paths of line of sight (LoS) and multipath components (MPCs) are drawn in red and blue, respectively. The propagation paths of the remaining network links are indicated in grey (LoS in dark grey and MPCs in light grey). The ground truth of the user's trajectory and his initial moving direction are indicated in green

paths. In Ref. [10], we have therefore introduced reflection sequences that describe the signal propagation for each MPC from the transmitting to receiving node, chronologically. Thereby, the surrounding environment is represented by a finite number of reflecting surfaces, which determine the set \mathcal{S} . For example, a quadratic room consists of four surrounding walls plus ceiling and floor. The corresponding set \mathcal{S} would thus comprise six reflecting surfaces, that is, $\mathcal{S} \in \{s_1, \dots, s_6\}$. Using tuple notation, the propagation path corresponding to MPC n of link l is thus expressed by the sequence $\xi_{l,n} = (s_b)$ with $s_b \in \mathcal{S}$. That is, if, for example, a signal is reflected twice on its way from the transmitter to the receiver, for example, first at surface s_1 and then at surface s_4 , we can express the propagation path by the sequence $\xi_{l,n} = (s_1, s_4)$. Note that the length of the sequence, denoted by $N_{\xi_{l,n}}$, is determined by the order of reflection. In the preceding example, the length, that is, the number of elements of the sequence $N_{\xi_{l,n}} = 2$ corresponds to the second order reflection described.

Following Ref. [14, 15], we can subsequently construct virtual nodes, that is, virtual transmitters (VTs) and virtual receivers (VRs), by mirroring the physical nodes according to the reflection sequences. Thus, the resulting locations of the virtual nodes for sequence $\xi_{l,n}$ are denoted by $\mathbf{r}_{\text{VT}_{l,n}}^{(u)}$ and $\mathbf{r}_{\text{VR}_{l,n}}^{(N_{\xi_{l,n}}-u)}$, where the index $u \in \{0, \dots, N_{\xi_{l,n}}\}$ is referring to equidistant (virtual) node pairs. The distances between these node pairs correspond to the length of the physical propagation path, and thus, to the delay of the MPC. For any node pair, that is, irrespective of index u , the length of the propagation path can be expressed as

where $\mathbf{r}_{\text{VT}_{l,n}}^{(0)}$ and $\mathbf{r}_{\text{VR}_{l,n}}^{(0)}$ refer to the physical transmitting and receiving nodes. Since the intersection points between the paths of related node pairs correspond to the physical reflection points, we can finally reconstruct the physical propagation paths geometrically similar to optical ray tracing [14].

In this work, we assume that all observable signal components, that is, the LoS component and MPCs, of the received signal modelled in Equation (2) are perfectly associated. That means, the MPCs of link l are represented by the reflection sequences $\xi_{l,n} \in \mathcal{X}_l^*$, where \mathcal{X}_l^* denotes the set of associated sequences. Combining the associated sequences for the whole network results in the union set $\mathcal{X}^* = \cup_l \mathcal{X}_l^*$. Eventually, the cardinality $|\mathcal{X}^*| = \sum_l N_l$ determines the amount of all signal components used for MDFL.

Note that the association of MPCs with the corresponding propagation paths is crucial, since MDFL relies on the location information contained in these propagation paths. Mis-associated MPCs could therefore even degrade the localisation performance. However, since the focus of this work is on evaluating Bayesian filter solutions for MDFL, we refrain from considering the effects of data association algorithms and assume perfect association as mentioned above.

2.2 | Parameter estimation

For localisation, the MDFL system exploits variations in the received power of signal components, which thus needs to be determined in the next step. For determining the received power of signal components, we first compute the corre-



the reflection sequences. Thus, the resulting locations of the virtual nodes for sequence $\xi_{l,n}$ are denoted by $\mathbf{r}_{\text{VT}_{l,n}}^{(u)}$ and $\mathbf{r}_{\text{VR}_{l,n}}^{(N_{\xi_{l,n}}-u)}$, where the index $u \in \{0, \dots, N_{\xi_{l,n}}\}$ is referring to equidistant (virtual) node pairs. The distances between these node pairs correspond to the length of the physical propagation path, and thus, to the delay of the MPC. For any node pair, that is, irrespective of index u , the length of the propagation path can be expressed as

$$d(\xi_{l,n}) = d_{l,n} = \|\mathbf{r}_{\text{VT}_{l,n}}^{(u)} - \mathbf{r}_{\text{VR}_{l,n}}^{(N_{\xi_{l,n}}-u)}\|, \quad (3)$$

sume perfect association as mentioned above.

2.2 | Parameter estimation

For localisation, the MDPL system exploits variations in the received power of signal components, which thus needs to be determined in the next step. For determining the received power of signal components, we first compute the corresponding amplitude values from the received signal. Given the delay $\bar{\tau}_{l,n}$ of the n th associated signal component of link l , we can calculate the amplitude as



$$\hat{\alpha}_{l,n}(t) = \int_0^{T_{\text{sym}}} \left(y_{l,n}^{\text{res}}(t) \right)^* s_l(t - \bar{\tau}_{l,n}) dt, \quad (4)$$

which represents the projection of the residuum signal $y_{l,n}^{\text{res}}(t)$ onto the transmit signal $s_l(t)$ [10, 14]. The residuum signal is determined by successively adjusting the received signal for the signal components up to the $(n - 1)$ -th, which can be expressed as

$$y_{l,n}^{\text{res}}(t) = y_l(t) - \sum_{n'=1}^{n-1} \hat{\alpha}_{l,n'}(t) s_l(t - \bar{\tau}_{l,n'}). \quad (5)$$

Using the square of the absolute value of the amplitude calculated in Equation (4), the measured power in the logarithmic domain can be expressed as

$$\hat{\gamma}_{l,n}(t) = 20 \log_{10} |\hat{\alpha}_{l,n}(t)|. \quad (6)$$

To measure variations in the received power, we need to know the absolute power level of each signal component. These power levels are determined during a system initialisation period [10]. Assuming the environment to be devoid of any mobile user, we compute the power values using Equations (4) and (6). By taking the mean over this period, we obtain the reference power level $\bar{\gamma}_{l,n}$.

For a discrete time step k , we can thus express the change in the power of a signal component by subtracting the reference power $\bar{\gamma}_{l,n}$ from the currently determined received power as

$$z_{l,n}(k) = \hat{\gamma}_{l,n}(k) - \bar{\gamma}_{l,n}. \quad (7)$$

Thus, the measurement vector $\mathbf{z}_k \in \mathbb{R}^{|\mathcal{X}^*|}$ can be composed by stacking the measured power changes for all links as

$$\mathbf{z}_k = [\dots, z_{l,n}(k), \dots]^T, \quad \forall l, n : \xi_{l,n} \in \mathcal{X}^*, \quad (8)$$

with $z_{l,n}(k)$ defined in dB.

2.3 | Measurement model

For applying MDFL, we require a model that relates the measured changes in the power of the signal components to the user state

$$\mathbf{x}_k = [\mathbf{r}_k^T, \mathbf{v}_k^T]^T, \quad (9)$$

including position \mathbf{r}_k and velocity \mathbf{v}_k of the user, that is, $\mathbf{h}(\mathbf{x}_k)$. Therefore, we model the measurement vector (8) as

$$\mathbf{z}_k = \mathbf{h}(\mathbf{x}_k) + \mathbf{w}_k, \quad (10)$$

assuming Gaussian measurement noise $\mathbf{w}_k \sim \mathcal{N}(\mathbf{0}, \mathbf{R})$ with a covariance matrix $\mathbf{R} \in \mathbb{R}^{|\mathcal{X}^*| \times |\mathcal{X}^*|}$ defined as

$$\mathbf{R} = \text{diag}(\dots, \sigma_{l,n}^2, \dots), \quad \forall l, n : \xi_{l,n} \in \mathcal{X}^*. \quad (11)$$

Note that to avoid complexity, we assume that the elements of the covariance matrix are independent of the user's location. Thus, the elements largely depend on the received power of the corresponding signal component.

Based on measurements, we have shown in Ref. [9] that user-induced variations in the power of MPCs can be modelled by superimposing the user impact on each pair of related virtual nodes. Similarly to Ref. [10], we approximate this impact on the individual node pairs using the empirical exponential model [6]. Thus, depending on the user location \mathbf{r}_k , we express changes in the power of any signal component, that is, the LoS component or MPC, corresponding to sequence $\xi_{l,n}$ in Equation (10) as the sum

$$h_{l,n}(\mathbf{x}_k) = \sum_{u=0}^{N_{\xi_{l,n}}} \phi_{l,n} e^{-\delta_{l,n}^{(u)}(\mathbf{r}_k)/\kappa_{l,n}}, \quad (12)$$

with the parameter $\phi_{l,n}$ as the maximum modelled power change in dB and $\kappa_{l,n}$ as the decay rate. The excess path length $\delta_{l,n}^{(u)}(\mathbf{r}_k)$ of the u th node pair is calculated by

$$\delta_{l,n}^{(u)}(\mathbf{r}_k) = \|\mathbf{r}_{\text{VT}_{l,n}}^{(u)} - \mathbf{r}_k\| + \|\mathbf{r}_{\text{VR}_{l,n}}^{(N_{\xi_{l,n}}-u)} - \mathbf{r}_k\| - d_{l,n}, \quad (13)$$

with path length $d_{l,n}$ as defined in Equation (3).

3 | BAYESIAN LOCALISATION APPROACHES

The localisation problem described in Section 2 can be formulated using the state–space representation: First, by a measurement model, which relates the measured power changes of signal components to the user state, as given in Equation (10) and second, by a transition model which describes the spatio-temporal evolution of the user state. In the literature, a common choice for the transition model is the white noise acceleration model [8, 16]. Therefore, the state equation is obtained as

$$\mathbf{x}_k = \mathbf{A}\mathbf{x}_{k-1} + \mathbf{n}_k, \quad (14)$$

with the transition matrix \mathbf{A} and zero-mean white Gaussian process noise \mathbf{n}_k with the covariance matrix \mathbf{Q} . The transition and covariance matrices are expressed as



$$\mathbf{A} = \begin{bmatrix} 1 & 0 & T_g & 0 \\ 0 & 1 & 0 & T_g \\ 0 & 0 & 1 & 0 \\ 0 & 0 & 0 & 1 \end{bmatrix}, \quad \mathbf{Q} = \sigma_p^2 \begin{bmatrix} \frac{T_g^3}{3} & 0 & \frac{T_g^2}{2} & 0 \\ 0 & \frac{T_g^3}{3} & 0 & \frac{T_g^2}{2} \\ \frac{T_g^2}{2} & 0 & T_g & 0 \\ 0 & \frac{T_g^2}{2} & 0 & T_g \end{bmatrix}, \quad (15)$$

where T_g is the time between two adjacent measurements and σ_p^2 is the process noise intensity of physical dimension $[\text{m}^2/\text{s}^3]$, which needs to be set according to application requirements [16]. The measurement and transition models can be expressed by the conditional probability density function (PDF) $p(\mathbf{z}_k | \mathbf{x}_k)$ and the transition prior distribution $p(\mathbf{x}_k | \mathbf{x}_{k-1})$, respectively.

The goal of sequential Bayesian estimation is to determine the PDF of the user state \mathbf{x}_k by computing the posterior density $p(\mathbf{x}_k | \mathbf{z}_{1:k})$ applying the general Bayesian update recursion [17]. A possible Bayesian approach for solving the non-linear system is the extended Kalman filter (EKF). The EKF linearises the system equations and approximates the posterior density with a Gaussian distribution. However, for the given localisation problem the density can hardly be assumed to be Gaussian. Thus, the EKF is likely to be unstable and to diverge (see Section 5.2.2). Note that also other advanced non-linear Bayesian filter solutions that rely on the assumption of a Gaussian posterior density, such as the posterior linearisation filter [18], would face similar problems as the EKF. In the following, we therefore present alternative filter solutions, which approximate the posterior with a non-parametric PDF and are thus more suitable for non-linear and non-Gaussian processes. In particular, we present the point mass filter (PMF) and the particle filter (PF), which use a deterministic and a stochastic grid, respectively, to approximate the posterior.

3.1 | Point mass filter

The PMF approximates the posterior distribution with the discrete density

$$p(\mathbf{x}_k | \mathbf{z}_{1:k}) \approx \sum_{i=1}^{N_s} w_{k|k}^i \delta(\mathbf{x}_k - \mathbf{x}^i), \quad (16)$$

where $\delta(\cdot)$ denotes the Dirac delta function and \mathbf{x}^i represents the i th grid point of the deterministic grid $\{\mathbf{x}^i\}_{i=1}^{N_s}$ [17]. The posterior weights are calculated by

with normalisation $c_k = \sum_{j=1}^{N_s} w_{k|k-1}^j p(\mathbf{z}_k | \mathbf{x}^j)$ and the likelihood distribution $p(\mathbf{z}_k | \mathbf{x}^i)$. The predicted weights are

$$w_{k|k-1}^i = \sum_{j=1}^{N_s} w_{k-1|k-1}^j p(\mathbf{x}^i | \mathbf{x}^j). \quad (18)$$

where $p(\mathbf{x}^i | \mathbf{x}^j)$ is the transition prior distribution applied to discretised grid points, which equals a multidimensional convolution [17]. Therewith, the complexity of the PMF grows quadratically with N_s .

3.2 | Particle filter

Also the PF approximates the posterior distribution with a discrete density

$$p(\mathbf{x}_k | \mathbf{z}_{1:k}) \approx \sum_{i=1}^{N_s} w_k^i \delta(\mathbf{x}_k - \mathbf{x}_k^i). \quad (19)$$

However, the PDF is approximated using a stochastic grid, that is, a set of weighted particles $\{\mathbf{x}_k^i\}_{i=1}^{N_s}$. Following the generic PF, the particles are drawn from an importance density [19]. Commonly this importance density is set equal to the transition prior distribution [17], which simplifies the weight update in the filter to

$$w_k^i = \frac{1}{c_k} w_{k-1}^i p(\mathbf{z}_k | \mathbf{x}_k^i), \quad (20)$$

with normalisation $c_k = \sum_{j=1}^{N_s} w_{k-1}^j p(\mathbf{z}_k | \mathbf{x}_k^j)$ and the likelihood distribution $p(\mathbf{z}_k | \mathbf{x}_k^i)$. Counteracting the problem of degeneracy, the PF applies resampling [19].

3.3 | Evaluation metric

For evaluating the localisation performance of the respective filter results, we use the root mean square error (RMSE) as a metric. In order to calculate the RMSE, we first determine a point estimate of the user state from the posterior densities of Equations (16) and (19) for PMF and PF, respectively, by calculating the weighted sum

$$\hat{\mathbf{x}}_k^{PMF} = \sum_{i=1}^{N_s} w_{k|k}^i \mathbf{x}^i \quad \text{and} \quad \hat{\mathbf{x}}_k^{PF} = \sum_{i=1}^{N_s} w_k^i \mathbf{x}_k^i, \quad (21)$$

which is the expected value of the posterior filter density. Based on the respective point estimate of the user state calculated in Equation (21), we can extract the location estimate $\hat{\mathbf{r}}_k$ for the PMF or the PF. Thus, we can finally compute the RMSE of the location estimate as



The PMF approximates the posterior distribution with the discrete density

$$p(\mathbf{x}_k | \mathbf{z}_{1:k}) \approx \sum_{i=1}^{N_k} w_{k|k}^i \delta(\mathbf{x}_k - \mathbf{x}^i), \quad (16)$$

where $\delta(\cdot)$ denotes the Dirac delta function and \mathbf{x}^i represents the i th grid point of the deterministic grid $\{\mathbf{x}^i\}_{i=1}^{N_k}$ [17]. The weights $w_{k|k}^i$ are calculated by

$$w_{k|k}^i = \frac{1}{c_k} w_{k|k-1}^i p(\mathbf{z}_k | \mathbf{x}^i), \quad (17)$$

calculating the weighted sum

$$\hat{\mathbf{x}}_k^{PMF} = \sum_{i=1}^{N_k} w_{k|k}^i \mathbf{x}^i \quad \text{and} \quad \hat{\mathbf{x}}_k^{PF} = \sum_{i=1}^{N_k} w_{k|k}^i \mathbf{x}_k^i, \quad (21)$$

which is the expected value of the posterior filter density. Based on the respective point estimate of the user state calculated in Equation (21), we can extract the location estimate $\hat{\mathbf{r}}_k$ for the PMF or the PF. Thus, we can finally compute the RMSE of the location estimate as

$$\text{RMSE}_k = \sqrt{E[\|\hat{\mathbf{r}}_k - \mathbf{r}_k\|^2]}, \quad (22)$$

where \mathbf{r}_k is the true user location.



4 | MEASUREMENT-BASED VERIFICATION OF THE NUMERICAL SIMULATION FRAMEWORK

In this section, we verify the applicability of a numerical simulation framework based on UWB measurement data for an indoor environment. We therefore first present the numerical simulation framework for time-variant power fluctuations. Then, we replicate the multipath propagation of the indoor measurement environment and simulate user-induced variations in the received power for each signal component following [9]. To assess the simulation framework, we finally compare the localisation performance of MDL using simulated data to the localisation performance of MDL using measured data.

4.1 | Numerical simulation framework

In the following, we present a numerical simulation framework for MDL, which enables a fast and flexible simulation of arbitrary propagation environments, network geometries, and user trajectories. Thereby, user-induced variations in the power of the signal components considered for MDL are determined numerically. This numerical simulation framework can be divided into three main steps:

1. The determination of the propagation environment, where we differentiate between fully artificial and replicated environments. For fully artificial environments, the propagation paths of MPCs are determined by the arbitrary arrangement of reflecting surfaces and thus by the resulting virtual nodes as introduced in Section 2.1. For replicated environments, the propagation paths are obtained in a similar way based on an existing floor plan using reflective surfaces, or by reusing previously determined propagation paths, as, for example, the propagation paths of Section 4.2.
2. The definition of a user trajectory, that is, a sequence of time-variant user positions \mathbf{r}_k . The distance between two successive user positions is determined by the velocity \mathbf{v}_k and the time between two adjacent measurement points T_g . Thereby, T_g is typically determined by the properties of the underlying communications system and the network dimensions.
3. The computation of user-induced variations in the power of signal components composing the measurement vector \mathbf{z}_k . We therefore apply the diffraction-based propagation model of Ref. [9] for each link and each considered signal component, as defined in the first step, for each position of the user trajectory, as defined in the second step. The variations in the power of signal components fundamentally depend on the dimensions of the user, the length of the propagation paths, and the carrier frequency f_c . The lengths of the propagation paths depend on the network geometry. The carrier frequency depends on the considered communications system. In this work, the user is modelled as an elliptical cylinder with a major axis of 0.55 m, a minor axis

of 0.25 m, and a height of 1.8 m. For further details on the propagation model, please refer to Ref. [9].

4.2 | Measurement setup

In order to assess the numerical simulation framework of Section 4.1, we deploy an UWB measurement system based on *Qorvo (DecaWave) DW1000* modules [20]. In particular, we set up a network consisting of one transmitting node and of $N_{\text{Rx}} = 7$ receiving nodes, as shown to scale in Figure 1, with all nodes at a height of 1 m above the ground. Note that the *Qorvo (DecaWave) DW1000* modules support IEEE 802.15.4a-based impulse UWB radio signals, and thus, the received signal corresponds to the CIR. In the following, we therefore refer to the received signal modelled in Equation (2) as CIR. Thus, the deployment of the UWB modules enables the continuous measurement of the CIRs for each network link. For measuring the CIR, the transmitting node individually addresses each receiving node in a round-robin manner initiating a two-way ranging procedure [20, 21]. The time between two adjacent measurements for the full network results in $T_g = 0.37$ s, cf. Table 1. Based on the measured CIRs we estimate the parameters for the signal components, that is, LoS and MPCs, which were previously determined during system initialisation [10]. For the experiment, we specifically consider 7 links in LoS and 13 links corresponding to MPCs, as indicated in Figure 1. Note that DFL considers only the propagation paths in LoS, while MDL considers the propagation paths of MPCs as additional network links. That means, the underlying network structures of DFL and MDL substantially differ. As specified in Equation (8), the measurement vector is composed of the measured power changes of all associated signal components within the network. Accordingly, the measurement vector for DFL comprises the power changes of the seven links in LoS, that is, $\mathbf{z}_k^{\text{DFL}} \in \mathbb{R}^7$, and the measurement vector for MDL comprises additionally the measured power changes of 13 MPCs, that is, $\mathbf{z}_k^{\text{MDL}} \in \mathbb{R}^{20}$. In this experiment, we aim at localising a single user who turned three rounds clockwise in the measurement environment. We recorded the ground truth using a Vicon high-precision optical motion

TABLE 1 Filter parameters—UWB experiment setup (Figure 1)

Parameter		Value		Unit
		PF	PMF	
Particles/grid points	N_s	1000	1113	
Grid point spacing	Δ_r	-	0.25	m
Measurement rate	T_g	0.37		s
Process noise intensity	σ_p^2	0.5		m^2/s^2
Measurement noise	$\sigma_{l,r}$	0.75		dB
Max. power change (12)	$\phi_{l,r}$	[-8.99, -0.95]		dB
Decay rate (12)	$\kappa_{l,r}$	[0.006, 0.131]		m

Abbreviations: PF, particle filter; PMF, point mass filter and; UWB, ultra-wideband.



capture system. For tracking, a reflector was attached to the head of the user. Thereby, the Vicon optical motion capture system allows to track the position of the reflector with a sub-centimetre accuracy. The corresponding ground truth trajectory together with the initial starting direction is illustrated in Figure 1.

4.3 | Assessment of the numerical simulation framework

The measured power variations of the UWB network presented in Section 4.2 now allow us to apply the PMF and the PF for localisation. Note that the resulting localisation performance serves as basis for the measurement-based evaluation of the numerical simulation framework introduced in Section 4.1. All parameters used for the filtering approaches are summarised in Table 1. Thereby, the PF is initialised by uniformly distributing the particle states within the observation area. Equivalently, the grid points of the PMF are arranged in an equidistant grid. For both filters, the weights are initially set equal.

Accounting for the stochastic nature of PFs, we have evaluated 100 realisations of the PF. Therefore, the presented RMSE results of the PF are determined by averaging over these realisations. Due to the deterministic grid, only one realisation is required for the PMF. An overview of the resulting mean RMSE values is provided in Table 2, including both DFL and MDFL using measured data.

For evaluating the applicability of the numerical simulation framework for MDFL, we additionally apply the PMF and the PF to simulated data. We therefore replicate the multipath propagation of the indoor environment of Section 4.2 and calculate the user-induced variations of the received power of all signal components for each position of the ground truth trajectory, cf. Figure 1. Note that the carrier frequency required for the simulation is set according to the UWB communications system, that is, $f_C = 3.9936$ GHz [20], and the time between two adjacent measurements is $T_g = 0.37$ s, see Table 1. Based on the simulated data, we eventually apply the PMF and the PF for localisation. Similarly to the filters applied to the measured data, we use the filter parameters from Table 1, initialise the PF by uniformly distributing the particle states within the observation area, and initially set the weights of the PMF equal. Accounting for measurement noise required for simulation, we have evaluated 500 realisations for each filter

solution. Therefore, all presented RMSE results using simulated data are determined by averaging over these realisations. The resulting mean RMSE values for both DFL and MDFL using simulated data are also given in Table 2, in addition to the results using measured data.

Finally, these localisation results obtained with measured and simulated data allow to assess the applicability of the numerical simulation framework. With a maximum difference of 0.05 m among all considered localisation approaches and network structures, the mean RMSE values show a very strong agreement. Moreover, Figures 2 and 3 show the cumulative distribution functions (CDFs) of the RMSE for the PF and the PMF, respectively, for using both measured and simulated data. Also for the CDF, we can observe a very strong agreement between the localisation results obtained with measured and simulated data. That strong agreement of the CDF curves is thereby observed independently of applying the PF or the PMF solution, as well as, of using DFL or MDFL. Therefore, this comparison has shown that the numerical simulation framework of Section 4.1 is able to sufficiently represent the

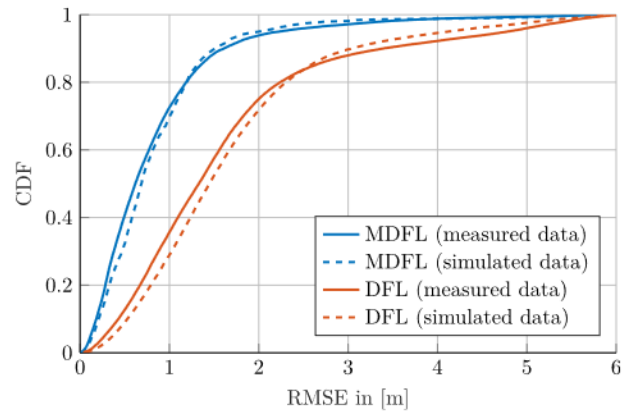


FIGURE 2 Cumulative distribution function (CDF) of the root mean square error (RMSE) of the location estimate for device-free localisation (DFL) and multipath-enhanced device-free localisation (MDFL) applying particle filter solution to both simulated and measured data

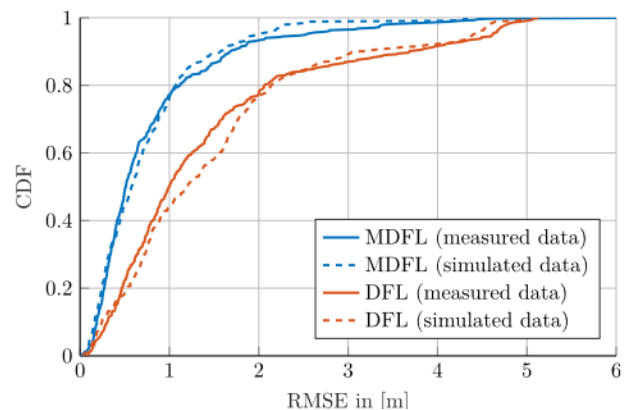


TABLE 2 Mean RMSE in (m)—UWB experiment setup (Figure 1)

Data	MDFL		DFL	
	PF	PMF	PF	PMF
Measured	0.83	0.79	1.64	1.44



within the observation area, and initially set the weights of the PMF equal. Accounting for measurement noise required for simulation, we have evaluated 500 realisations for each filter

TABLE 2 Mean RMSE in (m)—UWB experiment setup (Figure 1)

Data	MDFL		DFL	
	PF	PMF	PF	PMF
Measured	0.83	0.79	1.64	1.44
Simulated	0.82	0.74	1.68	1.49

Abbreviations: DFL, device-free localisation; MDFL, multipath-enhanced device-free localisation; PF, particle filter; PMF, point mass filter; RMSE, root mean square error; UWB, ultra-wideband.

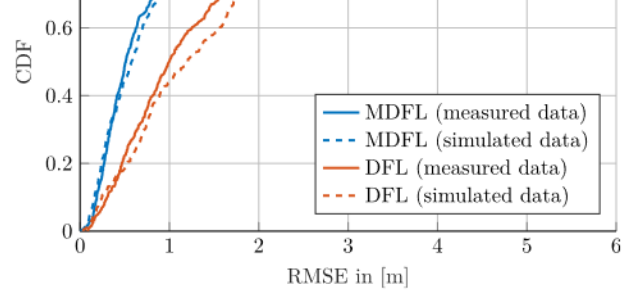


FIGURE 3 Cumulative distribution function (CDF) of the root mean square error (RMSE) of the location estimate for device-free localisation (DFL) and multipath-enhanced device-free localisation (MDFL) applying point mass filter solution to both simulated and measured data



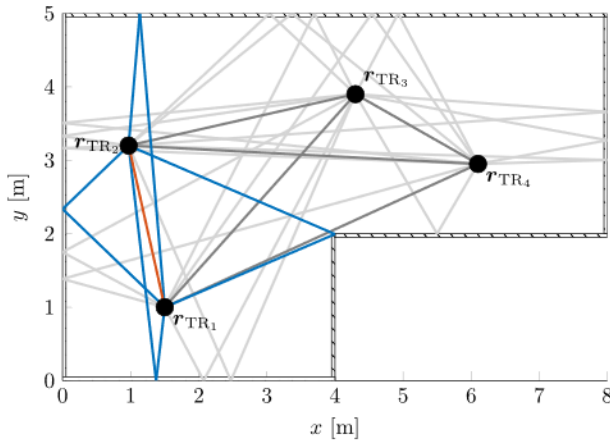


FIGURE 4 Exemplary multipath-enhanced device-free localisation network of four network nodes at locations $\mathbf{r}_{\text{TR}_{\{q\}}}$, $q = \{1, 2, 3, 4\}$. Reflecting surfaces of the surrounding environment are given by hatched lines. For the network link between $\mathbf{r}_{\text{TR}_{\{1\}}}$ and $\mathbf{r}_{\text{TR}_{\{2\}}}$ the multipath propagation is explicitly highlighted: physical propagation paths of the line of sight (LoS) and multipath components (MPCs) are red and blue. For the remaining network links, the propagation paths are indicated in grey (LoS in dark grey and MPCs in light grey)

propagation environment, which allows to obtain very comparable and thus realistic localisation results. Accordingly, the numerical simulation framework has been shown to be very well suited to provide the basis for a sound numerical evaluation of MDFL.

5 | PERFORMANCE EVALUATION

In this section, we discuss the localisation performance of DFL and MDFL based on measurements from the UWB experiment. For a sound analysis of the proposed non-linear Bayesian approaches, we additionally apply the simulation framework to evaluate the approaches numerically. Therefore, we first specify the simulation setup, that is, the network structure as well as the propagation environment, and define relevant trajectories for the evaluation. Finally, we analyse the numerical results.

5.1 | Measurement-based evaluation

An overview of the localisation performance for the UWB experiment is given in Table 2; see Section 4.3. The results on localisation performance show that both DFL and MDFL can be basically realised with a sparse network of commercial communications devices. With mean RMSE values of 0.83 m for the PF and 0.79 m for the PMF, MDFL thereby clearly outperforms DFL, for which mean RMSE values of 1.64 and 1.44 m are achieved for PF and PMF, respectively. Furthermore, the superiority in localisation performance of MDFL over DFL is particularly evident in the CDF curves of Figures 2 and 3 for PF and PMF. For the PF, the RMSE is in 80 % of the cases below approximately 1.2 m for MDFL and

2.2 m for DFL, cf. Figure 2. Similarly for the PMF, the RMSE is in 80 % of the cases below approximately 1.0 m for MDFL and 2.0 m for DFL, cf. Figure 3. Thus, regardless of the Bayesian filter solution, MDFL improves the localisation accuracy by approximately 1 m compared to DFL. Therewith, the localisation results obtained using measured data confirm the theoretical findings of Ref. [10], that considering MPCs for DFL improves the localisation performance.

Since the focus of this paper is on Bayesian localisation approaches, we compare the localisation performance of PF and PMF separately. For the considered trajectory both filtering solutions achieve a very comparable localisation performance, regardless of the underlying network, that is, for both DFL and MDFL. Note, however, that the evaluation of only one trajectory does not allow reliable conclusions about the respective aptitudes of the Bayesian localisation approaches. An elaborate evaluation requires a more detailed analysis that takes into account additional trajectories as well as different propagation environments. Since the numerical simulation framework presented in Section 4.1 can simulate arbitrary trajectories and propagation environments, it offers the opportunity to analyse the localisation algorithms in depth.

5.2 | Simulation-based evaluation

In the following, we apply the numerical simulation framework to identify and elaborate on the strengths and weaknesses of the considered Bayesian localisation algorithms. We therefore introduce an additional simulation environment representing a typical office space. The corresponding simulation setup and the numerical results are presented below.

5.2.1 | Simulation setup

The localisation approaches presented in Section 3 are evaluated in more detail using the numerical simulation framework of Section 4.1. In particular, we consider a fully meshed network of $N = 4$ collocated transmitting and receiving nodes. All nodes are located at the same height and correspond to the height of the body centre of the user. The multipath propagation environment is characterised by six reflecting surfaces that may represent a typical office space. The arrangement of the surfaces as well as the arrangement of the network nodes are shown to scale in Figure 4. Considering only first order reflections, the network consists of 6 links in LoS and 20 visible links corresponding to MPCs. Thus, according to Equation (8), the measurement vector for DFL contains the power changes of six links in LoS, that is, $\mathbf{z}_k^{\text{DFL}} \in \mathbb{R}^6$, and the measurement vector for MDFL contains additionally the power changes of 20 MPCs, that is, $\mathbf{z}_k^{\text{MDFL}} \in \mathbb{R}^{26}$. Using the numerical simulation framework of Section 4.1, we simulate user-induced variations in the power of signal components for four different user trajectories. The trajectories are shown in Figure 5 including starting point and moving direction. Based on the simulated user-induced power variations, we apply the PMF and the PF for localisation. All



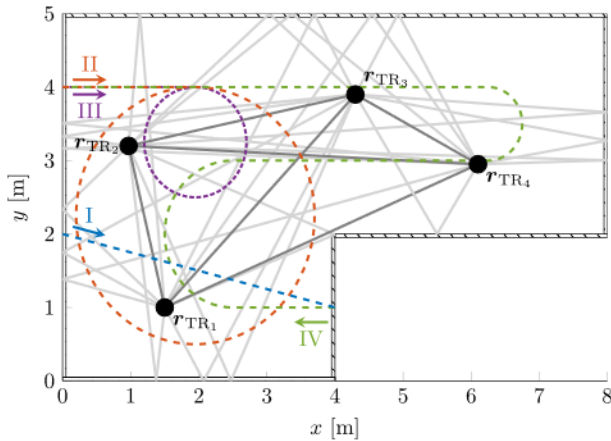


FIGURE 5 Simulation trajectories for different runs. The initial moving direction of each trajectory is indicated by coloured arrows. The underlying multipath-enhanced device-free localisation network is indicated in grey (see Figure 4)

TABLE 3 Filter parameters—Simulation setup (Figure 4)

Parameter		Value		Unit
		PF	PMF	
Particles/grid points	N_s	1000	3331	
Grid point spacing	Δ_r	-	0.1	m
Measurement rate	T_g	0.01		s
Process noise intensity	σ_p^2	0.1		m^2/s^2
Measurement noise	$\sigma_{i,n}$	0.75		dB
Max. power change (12)	$\phi_{i,n}$	[-8.91, -3.74]		dB
Decay rate (12)	$\kappa_{i,n}$	[0.016, 0.072]		m

Abbreviations: PF, particle filter; PMF, point mass filter.

parameters used for the filtering approaches are summarised in Table 3 and are applied for each trajectory. As in Section 4.3, the PF is initialised by uniformly distributing the particle states in the observation area, the PMF by arranging the grid points in an equidistant grid, and the weights of both filters are initially set equal.

5.2.2 | Numerical results

For each trajectory we have evaluated 500 realisations accounting for measurement noise. The presented RMSE results are determined by averaging over these realisations. A summary of the individual filter performances is given in Table 4 providing the mean RMSE values for each trajectory. In addition to the proposed PMF and PF, we also show the results of an EKF solution (parameter settings similar to Table 3). In

TABLE 4 Mean RMSE in (m)—Simulation setup (Figure 4), trajectories as in Figure 5

Trajectory	MDFL			DFL		
	EKF	PF	PMF	EKF	PF	PMF
I	1.01 ^a	0.25	0.28	-	1.93	1.82
II	4.72 ^a	0.84	0.62	-	2.43	2.29
III	2.33 ^a	1.08	0.75	-	1.99	1.80
IV	5.41 ^a	0.47	0.41	-	1.08	1.57
Overall	3.94 ^a	0.65	0.51	-	1.78	1.87

Abbreviations: DFL, device-free localisation; EKF, extended Kalman filter; MDFL, multipath-enhanced device-free localisation; PF, particle filter; PMF, point mass filter and; RMSE, root mean square error.

^aEstimation strongly diverges.

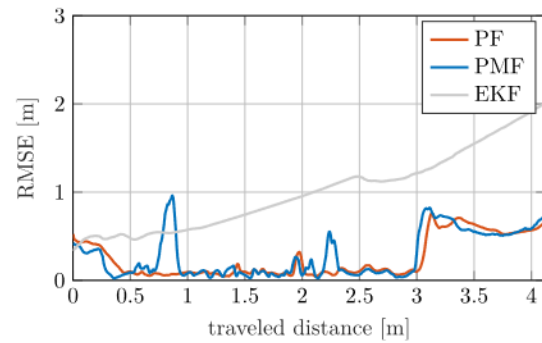


FIGURE 6 Root mean square error (RMSE) localisation performance of multipath-enhanced device-free localisation for different non-linear Bayesian filter solutions for Trajectory I. EKF, extended Kalman filter; PF, particle filter; PMF, point mass filter

can be explained by the sparse network configuration ($N = 4$ network nodes), which results in a non-Gaussian and often multimodal posterior density. In contrast, both PMF and PF could achieve stable results that significantly outperform the EKF for MDFL (see also Figure 6).

Figure 6 shows the RMSE results for Trajectory I using MDFL. Both PMF and PF achieve a sub-metre localisation performance over the entire trajectory, which also applies at the beginning of the trajectory. Due to the propagation paths of the MPCs, which are in the proximity of the starting point of Trajectory I (see Figure 5), the filters immediately obtain a good location estimate. Compared to the PF, the RMSE of the PMF slightly deviates at a travelled distance of 0.8 and 2.2 m. This deviation can be explained by local multimodalities of the posterior, which are resolved in this case by the PF due to resampling. After a travelled distance of 3 m, the RMSE increases for both PMF and PF. Due to the network structure, the trajectory lies after this point in a blank area that is not touched by any propagation path and the user does not induce any perturbations. Thus, the estimated posterior spreads over



For each trajectory we have evaluated 500 realisations accounting for measurement noise. The presented RMSE results are determined by averaging over these realisations. A summary of the individual filter performances is given in Table 4 providing the mean RMSE values for each trajectory. In addition to the proposed PMF and PF, we also show the results of an EKF solution (parameter settings similar to Table 3). In Ref. [8], the EKF is used as benchmark system for DFL; however, we could not obtain reasonable results for DFL and only unstable and diverging results for MDFL, even though the EKF was initialised ideally. The poor performance of the EKF

good location estimate. Compared to the PF, the RMSE of the PMF slightly deviates at a travelled distance of 0.8 and 2.2 m. This deviation can be explained by local multimodalities of the posterior, which are resolved in this case by the PF due to resampling. After a travelled distance of 3 m, the RMSE increases for both PMF and PF. Due to the network structure, the trajectory lies after this point in a blank area that is not touched by any propagation path and the user does not induce any perturbations. Thus, the estimated posterior spreads over that blank area, here, between $x \in (2.5 \text{ m}, 4 \text{ m})$ and $y \in (0 \text{ m}, 2 \text{ m})$.

The starting points of Trajectories II and III are also located in a blank area (see Figure 5). As shown in the results



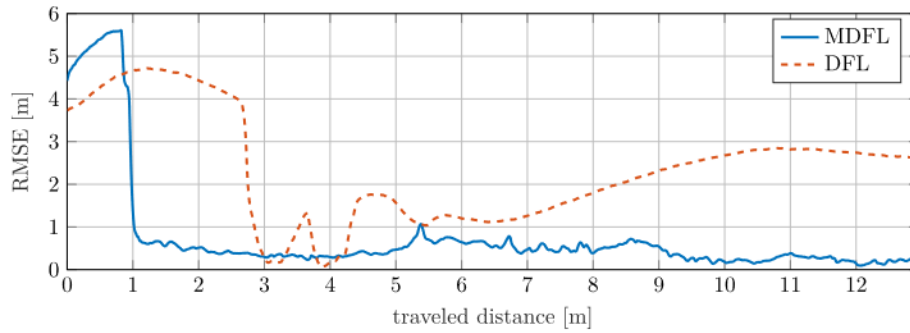


FIGURE 7 Root mean square error (RMSE) localisation performance of device-free localisation (DFL) and multipath-enhanced device-free localisation (MDFL) both applying the particle filter solution for Trajectory II

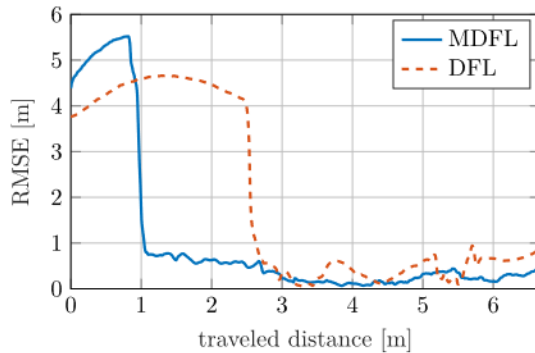


FIGURE 8 Root mean square error (RMSE) localisation performance of device-free localisation (DFL) and multipath-enhanced device-free localisation (MDFL) both applying the particle filter solution for Trajectory III

of the PF in Figures 7 and 8, no user-induced perturbations can be measured initially and thus the PDF spreads over the entire observed area. An accurate position estimate is only obtained when the user induces perturbations in the power of any network link, which is the case for MDFL after 1 m and for DFL after almost 3 m. In addition to the initial phase, also the comparison of the further course of Trajectories II and III give indication for the spatial localisation capabilities of DFL and MDFL. While we obtain a sub-metre localisation performance for MDFL almost entirely over both trajectories, the RMSE results for DFL strongly deviate for Trajectory II. The course of Trajectory II is mostly outside the DFL network and thus the user does not impact the signal propagation in LoS. For Trajectory III, also the DFL approach achieves localisation performance of less than 1 m, but is still outperformed by MDFL on average.

As shown in Figure 5, Trajectory IV is the longest scenario leading through the whole observation area. On average, the localisation performance is therefore only weakly distorted by initialisation and local geometric effects. With a mean RMSE of 0.41 m (PMF) and 0.47 m (PF), as given in Table 4, both filters achieve a very similar localisation performance for MDFL. For DFL, the performance of the PMF degrades to 1.57 m and of the PF to 1.08 m. Therewith, the PF outperforms the PMF in this specific scenario. Due to the very

sparse DFL network, the posterior density is more likely to be multimodal. Here, the PF could correctly resolve these multimodalities. If the PF would resolve for the wrong mode, the filter would diverge. However, the deterministic grid of the PMF completely avoids divergence.

6 | CONCLUSION

In this paper, we have presented the PMF and the PF as non-linear Bayesian filter solutions for DFL and MDFL. Using a network of commercial off-the-shelf UWB devices, we have applied the filter solutions to an indoor scenario and successfully demonstrated the applicability of MDFL through measured data. On the basis of these measurement results, we have derived and verified a numerical simulation framework, which allows a fast and flexible simulation of arbitrary propagation environments, network geometries, and user trajectories. Employing the numerical simulation framework, we have evaluated the filter solutions in detail using a sparse network comprising four collocated transmitting and receiving nodes. Regardless of the filter solution, the results show that MDFL outperforms DFL in localisation accuracy. For MDFL, the localisation performance of the proposed filters is comparable. We have shown that the localisation performance of both PMF and PF strongly depends on the underlying network structure and the corresponding density of propagation paths within the observation area. For the exemplary simulation environment, we have shown that both PMF and PF achieve a similar localisation performance below 1 m in most cases. Decisive factors for the choice of the filter are complexity on the one hand and probability of divergence on the other hand. For spatially large observation areas, the PMF may be prohibitive due to the quadratic growth in complexity. For very sparse networks, the PF may resolve for the wrong modes and, thus, diverges. However, for normal office rooms and a moderate number of network nodes, both filter solutions shall provide very accurate location estimates.

ACKNOWLEDGEMENT

None. Open access funding enabled and organized by Projekt DEAL.



CONFLICT OF INTEREST

The authors have declared no conflict of interest.

PERMISSION TO REPRODUCE MATERIALS FROM OTHER SOURCES

None.

DATA AVAILABILITY STATEMENT

Research data are not shared.

ORCID

Martin Schmidhammer  <https://orcid.org/0000-0002-9345-142X>

REFERENCES

- Sand, S., Dammann, A., Mensing, C.: Positioning in Wireless Communications Systems. John Wiley & Sons (2014)
- MarketsandMarkets: Indoor Location Market—Global Forecast to 2026. Online (2021). <https://www.marketsandmarkets.com/Market-Reports/indoor-location-market-989.html>
- IEEE 802 LAN/MAN Standards Committee: IEEE Standard for Information technology—Telecommunications and information exchange between systems Local and metropolitan area networks—Specific requirements—Part 11: Wireless LAN Medium Access Control (MAC) and Physical Layer (PHY) Specifications. IEEE Std 80211-2016 (Revision of IEEE Std 80211-2012). 1–3534 (2016)
- Kasher, A.: WiFi Sensing Use Cases. Online (2021). <https://mentor.ieee.org/802.11/dcn/20/11-20-1712-02-00bf-wifi-sensing-use-cases.xlsx>
- Patwari, N., Wilson, J.: RF sensor networks for device-free localization: measurements, models, and algorithms. *Proc. IEEE*. 98(11), 1961–1973 (2010). <https://doi.org/10.1109/jproc.2010.2052010>
- Guo, Y., et al.: An exponential-Rayleigh model for RSS-based device-free localization and tracking. *IEEE Trans. Mobile Comput.* 14(3), 484–494 (2015). <https://doi.org/10.1109/tmc.2014.2329007>
- Lei, T., et al.: Enhanced geometric filtering method based device-free localization with UWB wireless network. *IEEE Trans. Veh. Technol.* 70(8), 7734–7748 (2021). <https://doi.org/10.1109/tvt.2021.3090433>
- Kaltiokallio, O., Hostettler, R., Patwari, N.: A novel Bayesian filter for RSS-based device-free localization and tracking. *IEEE Trans. Mobile Comput.* 20(3), 780–795 (2021). <https://doi.org/10.1109/tmc.2019.2953474>
- Schmidhammer, M., et al.: Physical modeling for device-free localization exploiting multipath propagation of mobile radio signals. In: Proc 14th European Conference on Antennas and Propagation (EuCAP 2020) (2020)
- Schmidhammer, M., et al.: Multipath-enhanced device-free localization in wideband wireless networks. *IEEE Antenn. Wireless Propag. Lett.* 20(4), 453–457 (2021). <https://doi.org/10.1109/lawp.2021.3052438>
- Schmidhammer, M., et al.: Bayesian approaches to multipath-enhanced device-free localization. In: 2021 15th European Conference on Antennas and Propagation (EuCAP 2021) (2021)
- Molisch, A.F.: Ultra-wide-band propagation channels. *Proc. IEEE*. 97(2), 353–371 (2009). <https://doi.org/10.1109/jproc.2008.2008836>
- Bello, P.: Characterization of randomly time-variant linear channels. *IEEE Trans. Commun. Syst.* 11(4), 360–393 (1963). <https://doi.org/10.1109/tcom.1963.1088793>
- Meissner, P., Leitinger, E., Witrisal, K.: UWB for robust indoor tracking: weighting of multipath components for efficient estimation. *IEEE Wirel. Commun. Lett.* 3(5), 501–504 (2014). <https://doi.org/10.1109/lwc.2014.2341636>
- Gentner, C., et al.: Multipath assisted positioning with simultaneous localization and mapping. *IEEE Trans. Wireless Commun.* 15(9), 6104–6117 (2016). <https://doi.org/10.1109/twc.2016.2578336>
- Bar-Shalom, Y., Li, X., Kirubarajan, T.: Estimation with Applications to Tracking and Navigation: Theory, Algorithms and Software. John Wiley & Sons (2004)
- Gustafsson, F.: Particle filter theory and practice with positioning applications. *IEEE Aero. Electron. Syst. Mag.* 25(7), 53–82 (2010). <https://doi.org/10.1109/maes.2010.5546308>
- García-Fernández, A., et al.: Posterior linearization filter: principles and implementation using sigma points. *IEEE Trans. Signal Process.* 63(20), 5561–5573 (2015). <https://doi.org/10.1109/tsp.2015.2454485>
- Arulampalam, M.S., et al.: A tutorial on particle filters for online nonlinear/non-Gaussian Bayesian tracking. *IEEE Trans. Signal Process.* 50(2), 174–188 (2002). <https://doi.org/10.1109/78.978374>
- Decawave: DW1000 User Manual—How to Use, Configure and Program the DW1000 UWB Transceiver. User Manual version 2.18 (2017)
- Karásek, R., Gentner, C.: Stochastic data association for multipath assisted positioning using a single transmitter. *IEEE Access*. 8, 46735–46752 (2020). <https://doi.org/10.1109/access.2020.2977558>

How to cite this article: Schmidhammer, M., et al.: Bayesian multipath-enhanced device-free localisation: simulation- and measurement-based evaluation. *IET Microw. Antennas Propag.* 16(6), 327–337 (2022). <https://doi.org/10.1049/mia2.12244>



